JOURNAL OF GUIDANCE, CONTROL, AND DYNAMICS
Vol. 31, No. 1, January–February 2008

# Integrated Sliding Mode Guidance and Control for a Missile with On–Off Actuators

Amir Koren* and Moshe Idan†
*Technion—Israel Institute of Technology, 32000 Haifa, Israel*
and
Oded M. Golan‡
*RAFAEL, 31021 Haifa, Israel*

DOI: 10.2514/1.31328

**A sliding mode controller was recently introduced for integrated guidance-control loops of agile missiles. The sliding surface was chosen to be the zero-effort miss distance. This work extends this result to address nonlinear on–off actuators commonly used in such interceptors. The performance of the integrated design is compared with a two-loop design, that is, separate guidance and autopilot loops. The simulation includes a detailed pneumatic model of the aerodynamic surface actuators. Compared to the results obtained with a linear first-order actuation system, it is shown that the advantages of the integrated design are more significant when tested with the on–off actuator. The proposed integrated algorithm is effective especially for the end-game phase of the interception. However, its high interception accuracy can be attained only if engaged from a limited range of initial conditions within the so-called region of attraction, thus posing performance requirements to the midcourse guidance system. This paper presents the regions of attraction for a sample interception setup.**

## I. Introduction

FLIGHT control and guidance loops are commonly designed separately due to the assumption that there is a spectral separation between the two loops. The guidance system generates an acceleration command to the flight control logic. Consequently, the autopilot maneuvers the missile by actuating the aerodynamic control surfaces. At the end-game phase of the interception, the spectral separation assumption is often no longer valid due to fast relative geometry changes. This results in early command saturation that affects the interception performance.

An integrated guidance-control design may improve the end-game performance of the interceptor by accounting for the coupling between the control and guidance dynamics. Potentially, such a design may lead to smaller miss distances. This can favorably reduce the warhead size of future interceptors without affecting the interception effectiveness.

The improved performance attained by an integrated guidance-control design has been investigated by many researchers while using different control design techniques [1–5]. In [1], a game theoretic approach was used for the design of an integrated linear autopilot-guidance controller that minimizes the interception miss distance and the control energy of the interceptor. The state-dependent Riccati differential equation approach was used in [2]. Using a nonlinear 6 degrees of freedom simulation it was shown that the integrated controller provides improved miss distance statistics compared to the conventional two-loop design. The linear-quadratic-regulator approach coupled with the feedback linearization method was used in [3] for the design of an integrated controller. Recently, the sliding mode control (SMC) design approach was used for an integrated design for interceptors with single [4] and dual (canard and tail) [5] control surface configurations, demonstrating superior performance compared to the two-loop designs.

All of the above mentioned works show that the use of an integrated design leads to improved interception performance. This improvement is achieved by addressing the coupled nonlinear interception problem, involving both nonlinear kinematics and dynamics.

The coupled guidance-control design has to account for the inherent uncertainties of the end-game interception problem, resulting from unknown target maneuvers and interceptor modeling errors. Therefore, the design has to be addressed by a robust nonlinear control methodology. The SMC that is an intuitive and simple robust nonlinear control design technique was used for this problem in [4]. The SMC methodology was selected for the integrated design problem also because it was successfully used in several missile autopilot and guidance designs. For example, in [6], a high-order robust SMC missile autopilot was presented, designed to address the uncertainties in the nonlinear model of the missile dynamics. In [7], the SMC was used to derive a missile guidance law in the class of proportional navigation (PN). The sliding surface was selected to be proportional to the line of sight (LOS) rate, while the target maneuvers were considered as bounded uncertainties. Using numerical simulations, the superiority of the proposed guidance law over the conventional PN was advocated.

The integrated SMC design was based on somewhat simplified dynamics with a linear actuation model. In the current paper we extend this work for more realistic actuation dynamics. Specifically, we examine typical on–off actuation of air-to-air missiles using pneumatic actuators.

The pneumatic on–off actuator often leads to an oscillatory motion of the control surface around its commanded position. Because of system uncertainties, SMC controllers also exhibit nonlinear oscillations or chattering around the sliding surface, even when the system is linear. The goal of this study is to examine the effect of the oscillatory phenomena encountered when controlling an interceptor with on–off actuators with an integrated SMC controller on the interception accuracies.

This paper is organized as follows. In Sec. II we briefly review the SMC design methodology and present how it will be used for the

Presented as Paper 6788 at the AIAA Guidance, Navigation, and Control Conference, Keystone, Colorado, 21–24 August 2006; received 30 March 2007; revision received 13 August 2007; accepted for publication 17 August 2007. 

*Graduate Student, Faculty of Aerospace Engineering; korenamir@yahoo.com.
†Associate Professor, Faculty of Aerospace Engineering; moshe.idan@technion.ac.il. Associate Fellow AIAA.
‡Chief Systems Engineer, Post Office Box 2250, Department M5; omgolan@yahoo.com. Senior Member AIAA.

integrated guidance and control problem. Nonlinear and linear interception models that are used for the numerical simulation analysis and the integrated design, respectively, are discussed in Sec. III. The integrated and, for comparison, two-loop guidance and autopilot designs are given in Sec. IV. Performance evaluation and a comparison between the two designs, demonstrating the clear advantage of the integrated one, are given in Sec. V. The analysis also includes the set of initial conditions (the region of attraction) that guarantee high interception accuracy for the integrated design. Concluding remarks are offered in Sec. VI.

## II. Design Methodology

As advocated earlier, in this study the SMC methodology is used to design guidance, control, and integrated guidance-control algorithms for the end-game phase of an interception task. This work extends the results presented in [4] by addressing interceptors with pneumatic on–off actuators. In this section we briefly review the SMC methodology and outline its application to the integrated guidance and control design problem.

The SMC methodology is described in many papers and textbooks [8,9]. It is a nonlinear robust control design approach that can guarantee stability and performance of a dynamic system in the presence of modeling errors and uncertainties. The design simplicity is attained by converting a tracking problem of an $n$th-order dynamical system into a first-order stabilization problem [9].

The SMC controller is designed so that the system tracking error reaches a sliding surface or manifold, defined as a function of the system tracking error and possibly its derivatives. The number of derivatives used to define the sliding surface is dictated by the relative degree of the system output with respect to its control input. The sliding surface is chosen such that once the tracking error is forced to stay on it, the system will exhibit the desired dynamic response and tracking characteristics. In the guidance and control context the sliding surface is defined to attain interception. When not on the sliding surface, a control action is applied so as to reach this surface in a finite time. Because of unknown target maneuvers and system uncertainties, even if the sliding surface is reached, maintaining the tracking error on the sliding surface cannot be guaranteed. A repeated departure from and return to the sliding surface, the so-called chattering mode, may have an undesirable effect on the performance. Various smoothing techniques can be used to reduce the chattering by slightly compromising tracking accuracy.

The performance of the SMC controller is affected greatly by the sliding surface selection. One of the common options for a guidance related sliding surface is the LOS rate, motivated by the desire to attain a collision triangle with the target. If the interceptor and the target move at a constant speed, this would lead to the well-known PN guidance law. This law could turn out to be insufficient when addressing maneuvering targets.

Following [4], in the current work we chose the zero-effort miss (ZEM) [10] distance to be the sliding variable. The ZEM is commonly used in advanced optimal control and differential game formulations of guidance problems. In two-sided differential game problems, ZEM is the miss distance attained if, from the current time onward, both players do not apply control commands. It is computed by solving the associated homogenous engagement equations of motion. Using a high-order nonlinear model for the evaluation of the ZEM leads to a complex controller. Thus, for the controller synthesis, the ZEM is approximated using a simplified linear model. A robust SMC controller is then designed to address both the system uncertainties and the difference between the nonlinear and the linear design models.

## III. Interception Model

In this work we consider a roll stabilized canard controlled missile, addressing its dynamics in two perpendicular planes: longitudinal (vertical) and lateral (horizontal). The investigation is limited to the end-game phase of an interception problem. During this phase, we assume that the missile is close to a collision course and that the motion in the two planes is independent. Therefore, we present the interception kinematics and dynamics in only one (longitudinal/vertical) plane, thus addressing the problem as planar.

In the following paragraphs we present nonlinear dynamic models that are implemented in a numerical simulation used to analyze and compare the different guidance and control designs. These models are then linearized for a simplified yet realistic definition of the sliding surfaces used in the control synthesis. The actual controller design then uses the full nonlinear models of the interception problem.

### A. Nonlinear Kinematics and Dynamics

A nonlinear kinematics and dynamics model will be used to simulate the end game of a planar interception and used in the controller design. A view of the planar end-game geometry, depicted on a $X_I$–$O_I$–$Z_I$ Cartesian initial reference frame, is shown in Fig. 1. The $M$ and $T$ subscripts represent the missile and the target, respectively. $V$, $a$, and $\gamma$ denote the speed, normal acceleration, and flight path angle, respectively. $r$ is the range between the missile and the target, and $\lambda$ is the angle between the temporal and initial LOS directions. We choose the $X_I$ axis of the Cartesian inertial frame to be aligned with the initial LOS direction. This choice of coordinates leads to a zero initial LOS angle, that is, $\lambda_0 = 0$. $a_{MN}$ and $a_{TM}$ are, respectively, the missile and target acceleration components perpendicular to the LOS.

The engagement kinematics are expressed in a polar coordinate system $(r, \lambda)$ attached to the missile. Neglecting the gravitation force, the kinematics are given by

$$\dot{r} = V_r \tag{1}$$

$$\dot{\lambda} = V_r / r \tag{2}$$

Here, $V_r$ is the closing speed given by

$$V_r = -[V_M \cos(\gamma_M - \lambda) - V_T \cos(\gamma_T - \lambda)] \tag{3}$$

and $V_\lambda$ is the speed perpendicular to the LOS

$$V_\lambda = -V_M \sin(\gamma_M - \lambda) + V_T \sin(\gamma_T - \lambda) \tag{4}$$

In the sequel we will use the variable time to go $t_{go}$ that can be approximated by

$$t_{go} = -r / V_r \tag{5}$$

We assume that the target has first-order dynamics and is moving at a constant velocity. This is expressed by

$$\dot{\gamma}_T = a_T / V_T \tag{6}$$

$$\dot{a}_T = \left(a_T^c - a_T\right) / \tau_T \tag{7}$$

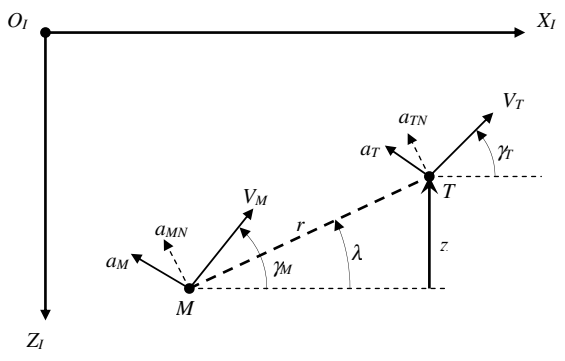


**Fig. 1 Planar engagement geometry.**

$\tau_T$ is the time constant of the target dynamic and $a_T^c$ is its maneuver command.

Figure 2 depicts the missile body-fixed rotating coordinate frame $X_{Mr} - M - Z_{Mr}$ used to express the missile planar dynamics. In this frame, $X_{Mr}$ is aligned with the missile longitudinal axis. Several variables used to model the missile dynamics are defined in the coordinate frame $X_{Mf} - M - Z_{Mf}$, also depicted in Fig. 2. This coordinate frame is parallel to the inertial frame $X_I$–$O_I$–$Z_I$ with its origin attached to the missile's center of gravity. The missile angle of attack and its pitch attitude angle are denoted by $\alpha$ and $\theta$, respectively. They are related to the flight path angle $\gamma_M$ by

$$\theta = \alpha + \gamma_M \tag{8}$$

Using the definitions in Fig. 2, the planar missile dynamics can be expressed as

$$\dot{V}_M = [T\cos\alpha - D(\alpha, \delta)]/m \tag{9a}$$

$$\dot{\alpha} = q - [T\sin\alpha + L(\alpha, \delta)]/(mV_M) \tag{9b}$$

$$\dot{q} = M(\alpha, q, \delta)/I \tag{9c}$$

$$\dot{\theta} = q \tag{9d}$$

where $q$ is the missile pitch rate, $m$ is its mass, $I$ the moment of inertia, and $\delta$ is the canard deflection angle. The dynamics of the canard will be detailed in Sec. III.B. $L$, $D$, and $M$ are, respectively, the aerodynamic lift, drag, and pitch moment acting on the missile. $L$ and $M$ are assumed positive when their action is to increase the flight path and pitch angles. The drag force $D$ is acting in the opposite direction of the velocity vector. Finally, $T$ is the missile engine thrust, assumed to be aligned with the $X_{Mr}$ axis. Because we consider the interception end game only, the engine is assumed to be off and the drag force to be negligible. Therefore, for the end-game phase, we assume that the missile velocity is constant, that is, $V_M = \text{const}$, thus further simplifying the model in Eqs. (9).

The total aerodynamic forces depicted in Fig. 3 and moments generated by the body and the canard are assumed to be proportional to the local angles of attack. The resulting aerodynamic lift and pitch moment, used in Eqs. (9) are modeled as

$$L/m = L_\alpha^B f(\alpha) + L_\alpha^\delta f(\alpha + \delta) \tag{10}$$

$$M/I = M_\alpha^B f(\alpha) + M_q q + M_\alpha^\delta f(\alpha + \delta) \tag{11}$$

where $f$ represents the nonlinear aerodynamic characteristics of the body and canard. In this work we introduce only the stall characteristics, approximated by a standard saturation function

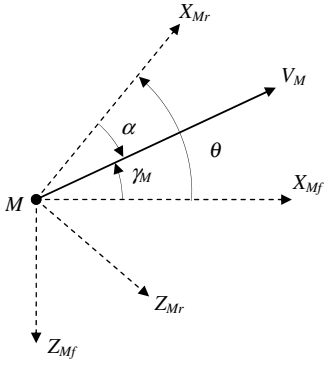


**Fig. 2 Missile coordinate systems.**

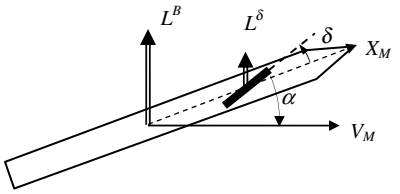


**Fig. 3 Aerodynamic forces acting on the missile.**

$$f(u) = \begin{cases} U_{\max} & U_{\max} < u \\ u & -U_{\max} \le u \le +U_{\max} \\ -U_{\max} & u < -U_{\max} \end{cases} \tag{12}$$

where $U_{\max}$ is the saturation limit.

### B. Pneumatic Actuator Model

Short range air-to-air missiles commonly use pneumatic actuators to control their aerodynamic surfaces. This is due to the high power-to-weight ratio of pneumatic systems compared to, for example, low power-to-weight electric systems. In this section we present a typical pneumatic actuator model. A schematic representation of the system is shown in Fig. 4.

We consider a setup where two pistons mounted in two cylinders are used to control the movement of the aerodynamic surface. During operation, one of the cylinders is charged while the other is discharged at all times. Each cylinder has an inlet and outlet nozzle; either one must be opened at any time. This type of operation generates a continuously fluctuating actuation moment on the aerodynamic control surface, causing it to oscillate.

The kinematics equation of the aerodynamic surface motion is given by

$$I_\delta \ddot{\delta} + K_{\dot{\delta}} \dot{\delta} + K_\delta(\delta + \alpha) = M_p \tag{13}$$

Here $I_\delta$ is the moment of inertia of the surface, $\delta$ is its rotation angle, $\alpha$ is the missile angle of attack, $K_\delta$ is the aerodynamic moment coefficient, and $K_{\dot{\delta}}$ is the viscosity coefficient. The moment $M_p$ produced by the two pistons actuating the surface is

$$M_p = P_1 Ad - P_2 Ad = (P_1 - P_2)Ad \tag{14}$$

where $A$ is the piston cross-section area and $d$ is the arm length. The gas in the cylinder is assumed to be ideal, complying with the ideal gas equation

$$pV = mRT \tag{15}$$

$p$ is the gas pressure in the cylinder, $V$ is the gas volume, $m$ is the gas mass, $R$ is the gas constant, and $T$ is the gas temperature.

To model the gas dynamics in the cylinder, we need to define the thermodynamic relation between its temperature and pressure during the cylinder charge and discharge. Common simplifying assumptions could be that the process is either isentropic (adiabatic and reversible) or isothermal. Because the charge/discharge is very

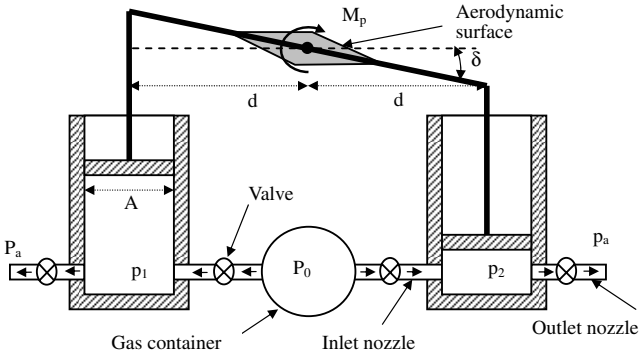


**Fig. 4 Schematic representation of the pneumatic actuator.**

fast, almost no heat will be transferred out of the cylinder. Thus the process could be adiabatic and not isothermal. On the other hand, because the discharge process is irreversible, it cannot be considered isentropic. Hence we conclude that the process is somewhere between isentropic and isothermal. Consequently, from a practical engineering standpoint, we assume that thermodynamically the process in the cylinders is polytropic [11,12]. The validity and the effect of this assumption on the interception accuracy will be evaluated numerically in the sequel.

In a polytropic process, the pressure and temperature are related by

$$\frac{T}{T_0} = \left(\frac{p}{p_0}\right)^{n-1/n} \tag{16}$$

where $n$ is the process constant, $p_0$ and $T_0$ are, respectively, the gas container pressure and temperature. The process constant is selected in the range $1 \le n \le \gamma$, with $\gamma = C_p/C_v$. When $n = 1$ the process is isothermal; for $n = \gamma$ it is isentropic.

Differentiating Eq. (15) while assuming a polytropic process, Eq. (16), leads to

$$\dot{p} = \frac{n}{V}\left[\dot{m}RT_0\left(\frac{p}{p_0}\right)^{(n-1)/n} - p\dot{V}\right] \tag{17}$$

The relations between the surface angle and the gas volume in the cylinders are

$$V_1 = Ad(\delta_0 + \delta) \quad \text{and} \quad V_2 = Ad(\delta_0 - \delta) \tag{18}$$

where $Ad\delta_0$ represents the gas volume in the cylinder at $\delta = 0$ deg and consequently specifies the maximum actuator range. In this work we chose $\delta_0 = \pi/4$, while allowing surface movement of about $\pm 30$ deg. Substituting the latter into Eq. (17), the pressure dynamics for the two cylinders can be expressed as

$$\begin{aligned} \dot{p}_1 &= \frac{n}{Ad(\pi/4 + \delta)}\left[\dot{m}_1 RT_0\left(\frac{p_1}{p_0}\right)^{(n-1)/n} - p_1 Ad\dot{\delta}\right] \\ \dot{p}_2 &= \frac{n}{Ad(\pi/4 - \delta)}\left[\dot{m}_2 RT_0\left(\frac{p_2}{p_0}\right)^{(n-1)/n} + p_2 Ad\dot{\delta}\right] \end{aligned} \tag{19}$$

The equations of the gas flow $\dot{m}$ into and from the cylinders are governed by the compressible airflow equations, and are presented separately for the charging and discharging cylinders. Charge and discharge are attained, respectively, through inlet and outlet nozzles of the two cylinders, controlled by valves that introduce a delay into the actuation process. The flow through the nozzles is assumed to be isentropic. Equations for the gas flow through the nozzles presented next were developed according to compressible fluid flow theory [13].

*Charging cylinder:* During cylinder charge there is no flow through the cylinder outlet nozzle while the inlet nozzle is open. The flow rate through the nozzle depends on the ratio between the pressures on the two sides of the nozzle. When the pressure in the cylinder is lower than a critical value, the flow in the nozzle reaches Mach one and becomes choked. The critical pressure that determines whether the flow is choked is given by

$$p_{\text{crit}} = p_0 \cdot \left(\frac{2}{\gamma + 1}\right)^{\gamma/\gamma - 1} \tag{20}$$

where $p_0$ is the pressure in the gas container. In this case, the gas flow equation is

$$\dot{m} = p_0 A_n \sqrt{\frac{\gamma}{RT_0}}\left(\frac{2}{1+\gamma}\right)^{1+\gamma/2(\gamma-1)} \tag{21}$$

where $A_n$ is the nozzle cross-section area. When $p > p_{\text{crit}}$, the flow through the nozzle is not choked, and the gas flow equation is

$$\dot{m} = p_0 A_n \frac{1}{\sqrt{RT_0}}\left[\left(\frac{p}{p_0}\right)^{\gamma/2} - \left(\frac{p}{p_0}\right)^{\gamma/\gamma+1}\right]^{1/2}\sqrt{\frac{2\gamma}{\gamma - 1}} \tag{22}$$

*Cylinder discharge:* During cylinder discharge there is no flow through the cylinder inlet nozzle and the gas trapped in the cylinder is released into the atmosphere. Because of the large difference between the pressure inside the cylinder and the atmospheric pressure, the flow through the outlet nozzle is assumed to be choked during the entire discharge phase. Hence, the gas flow equation will be

$$\dot{m} = -pA_n\sqrt{\frac{\gamma}{RT}}\left(\frac{2}{1+\gamma}\right)^{1+\gamma/2(\gamma-1)} \tag{23}$$

The following are typical parameters that were chosen to simulate the nonlinear pneumatic actuator: gas container parameters are $p_0 = 40$ atm and $T_0 = 295$ K; $A \cdot d = 7.4\text{e}-6$ m$^3$; for the charging valves $A_n = 6.75\text{e}-7$ m$^2$, while for the discharging valves $A_n = 5.11\text{e}-7$ m$^2$; valve actuation dynamics is modeled as pure time delay of 0.002 s; helium is the standard gas used in such actuators with $\gamma = 1.67$ and $R = 2078.6$ J/(Kg · K).

### 1. *Actuator Control System*

The pneumatic actuator is controlled by a dedicated control system. It switches between the charge and discharge phases of the cylinders according to the control surface command angle and its actual state, that is, surface angle and its rate. Typically, the switching function is selected as the sign of a linear combination of these quantities:

$$e^c = \text{sign}[(\delta^c \cdot K_{\text{sf}} - \delta)K_{\text{act1}} - \dot{\delta} \cdot K_{\text{act2}}] \tag{24}$$

The constants $K_{\text{act1}}$ and $K_{\text{act2}}$ determine the dynamic characteristics of the controlled pneumatic actuator, and, in particular, the frequency and amplitude of the actuator oscillation. $K_{\text{sf}}$ is a scale factor parameter introduced to reduce the average steady-state error of the actuator response to a step input command. This error is caused by the asymmetric characteristics of the charging and discharging cylinders. After fine-tuning the actuator step response, the control system parameters were set to $K_{\text{act1}} = 100$, $K_{\text{act2}} = 1$, and $K_{\text{sf}} = 1.09$.

### 2. *Approximate Linear Actuator Model*

Because of its complexity, the detailed pneumatic model will be used only in the nonlinear interception simulations. The controller design will be carried out assuming a first-order actuation model, that is,

$$\dot{\delta} = (\delta^c - \delta)/\tau_s + \Delta_\delta \tag{25}$$

where $\Delta_\delta$ is the modeling error between the pneumatic nonlinear model and the first-order approximation. We assume that this error is bounded

$$|\Delta_\delta| \le \bar{\Delta}_\delta \tag{26}$$

In Fig. 5 we compare the step responses of the linear and pneumatic actuators to a 25 deg deflection command. The missile is assumed to be fixed at a zero angle of attack. The time constant of the first-order model, that best fits the nonlinear model dynamics, was set to 0.01 s. The figure shows clearly the difference between the response of the first-order and the nonlinear pneumatic models. The most significant difference is the oscillatory behavior of the pneumatic actuator caused by its on–off operation mode. For the actuator parameters adopted in this study, the pneumatic model oscillates at approximately 40 Hz and amplitude of about 1.4 deg.

To further justify the first-order approximation of the nonlinear pneumatic actuator model, Fig. 6 compares the numerically computed describing function of the pneumatic model to the frequency response of the first-order model. The describing function

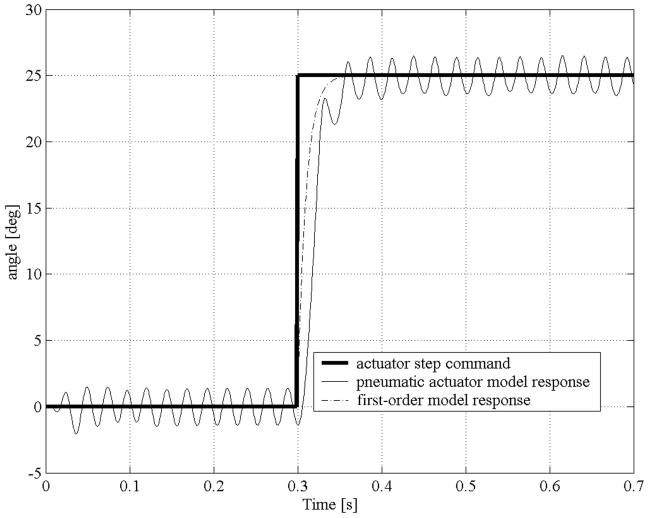


**Fig. 5 Step response of the pneumatic and first-order actuator models.**

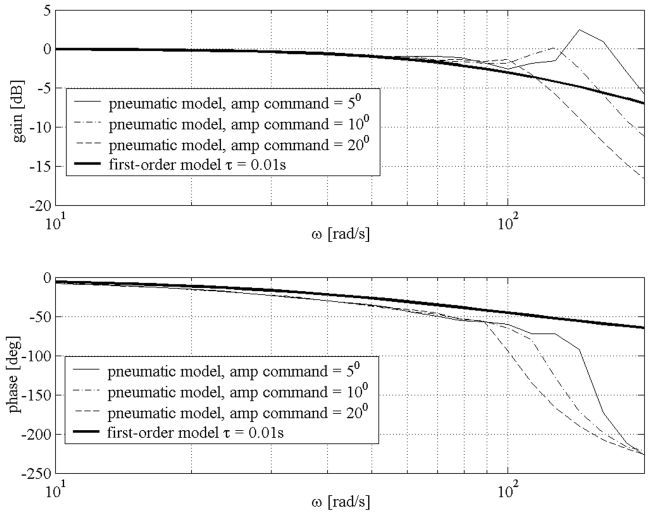


**Fig. 6 Describing the function for the pneumatic model and the frequency response of the approximate first-order actuator model.**

[9] is a frequency response method used to approximately analyze and predict the dynamic characteristics of a nonlinear system. In this work, the describing function was obtained by numerically simulating the pneumatic model response to a sinusoidal input and computing the ratio between the first harmonic of the output and the input. From Fig. 6 we conclude that for frequencies of up to 100 rad/s, the two models exhibit a similar behavior. At higher frequencies the two models depart. In addition, there is a difference between the frequency responses of the pneumatic model depending on the command amplitude. In the missile guidance and control context, these differences are not significant. The common practice is to design pneumatic actuators that oscillate at a significantly higher frequency than the controlled system bandwidth. Therefore, the agreement in the lower frequency range justifies the first-order approximation in the controller design process, while accounting for the modeling errors.

### C. Linearized Models

The full nonlinear model of the system presented above is too complex to define the ZEM sliding surface used in the proposed integrated guidance and control design. Thus, a simplified linear model for the kinematics, missile and target dynamics, and the actuator dynamics is used to define the ZEM. The other steps of the design presented in the sequel use the full nonlinear model. The linear kinematics and dynamics models, adopted from [4], are briefly outlined next.

#### 1. *End-Game Kinematics*

The state vector of the linearized guidance problem is defined by

$$x_G = \begin{bmatrix} z & \dot{z} & a_{TN} & a_{MN} \end{bmatrix}^T \tag{27}$$

Here, $z$ is the target-missile relative displacement normal to the initial LOS, $a_{TN}$ and $a_{MN}$ are, respectively, target and missile accelerations normal to the LOS. The latter are given by

$$a_{MN} = a_M \cos(\gamma_M - \lambda_0) \qquad a_{TN} = a_T \cos(\gamma_T - \lambda_0) \tag{28}$$

For the separate, two-loop guidance and autopilot design, that will be carried out for comparison, we assume that the dynamics of the missile controlled by an autopilot can be approximated by an equivalent first-order system with a time constant $\tau_M$. Using this assumption, the end-game kinematics with the approximated missile dynamics are given by

$$\dot{x}_G = A_G x_G + B_G a^c_{MN} + G_G a^c_{TN} \tag{29}$$

where

$$A_G = \begin{bmatrix} A_{G11} & A_{G12} \\ [0]_{1\times 3} & -1/\tau_M \end{bmatrix}, \qquad A_{G11} = \begin{bmatrix} 0 & 1 & 0 \\ 0 & 0 & 1 \\ 0 & 0 & -1/\tau_T \end{bmatrix}$$
$$A_{G12} = \begin{bmatrix} 0 \\ -1 \\ 0 \end{bmatrix} \tag{30}$$

$$B_G = \begin{bmatrix} 0 & 0 & 0 & 1/\tau_M \end{bmatrix}^T, \qquad G_G = \begin{bmatrix} 0 & 0 & 1/\tau_T & 0 \end{bmatrix}^T \tag{31}$$

Here $a^c_{TN}$ and $a^c_{MN}$ are, respectively, the target and missile acceleration commands normal to the initial LOS. In a two-loop design, $a^c_{MN}$ will be generated by the external guidance loop.

#### 2. *Missile Dynamics (Autopilot Loop)*

The linear missile dynamics, derived for a constant velocity flight and assuming a first-order canard actuator, are described using the state space vector

$$x_M = [\alpha \quad q \quad \delta]^T \tag{32}$$

Following Eq. (9), the linear model is given by

$$\dot{x}_M = A_M x_M + B_M \delta^c \tag{33}$$

where

$$A_M = \begin{bmatrix} -L_\alpha/V_M & 1 & -L^\delta_\alpha/V_M \\ M^B_\alpha & M_q & M^\delta_\alpha \\ 0 & 0 & -1/\tau_s \end{bmatrix}, \qquad B_M = \begin{bmatrix} 0 \\ 0 \\ 1/\tau_s \end{bmatrix} \tag{34}$$

$L_{(\cdot)}$ and $M_{(\cdot)}$ denote the dimensional control derivatives of the short period longitudinal missile model.

In the two-loop design, the outer guidance loop will require the missile acceleration normal to the initial LOS. The acceleration component is given by

$$a_{MN} = C_M x_M \tag{35}$$

where

$$C_M = \begin{bmatrix} L_\alpha & 0 & L^\delta_\alpha \end{bmatrix} \cdot \cos(\gamma_M - \lambda_0) \tag{36}$$

#### 3. *Integrated Dynamics*

The integrated kinematics and missile dynamics model combines the models presented above and is defined using the state space

vector

$$x_{GC} = [\, z \quad \dot{z} \quad a_{TN} \quad \alpha \quad q \quad \delta \,]^T \tag{37}$$

The model is given by

$$\dot{x}_{GC} = A_{GC} x_{GC} + B_{GC}\delta^c + G_{GC} a_{TN}^c \tag{38}$$

where

$$A_{GC} = \begin{bmatrix} A_{G11} & A_{12} \\ [0]_{3\times 3} & A_M \end{bmatrix}, \qquad A_{12} = \begin{bmatrix} [0]_{1\times 3} \\ -C_M \\ [0]_{1\times 3} \end{bmatrix} \tag{39}$$

$$B_{GC} = [\,[0]_{1\times 5} \quad 1/\tau_s\,]^T, \qquad G_{GC} = [\,0 \quad 0 \quad 1/\tau_T \quad 0 \quad 0 \quad 0\,]^T \tag{40}$$

The matrices $A_{G11}$, $A_M$, and $C_M$ were defined previously in Eqs. (30), (34), and (36), respectively.

### D. Zero-Effort Miss

The SMC methodology will be used for integrated and two-loop designs of the interceptor control logic, with ZEM defining the sliding variable. ZEM is the homogeneous solution of the engagement equations. It depends on the interception time (or time to go). ZEM cannot be easily computed for the complex nonlinear models presented in Secs. III.A and III.B. Therefore, we will approximate it using the linearized models of Sec. III.C.

For the separated guidance problem, let $\phi_G(t_f, t)$ be the transition matrix associated with the kinematics Eq. (29). It is given by

$$\phi_G(t_f, t) = \phi_G(t_{\text{go}}) = \exp(A_G t_{\text{go}}) \tag{41}$$

Consequently, the guidance ZEM is computed as

$$Z_G = C_G \phi_G(t_{\text{go}}) x_G \tag{42}$$

where

$$C_G = [\,1 \quad 0 \quad 0 \quad 0\,] \tag{43}$$

When addressing the integrated guidance-control problem, the associated ZEM is computed using the linear model of Eq. (38). In this case, it is given by

$$Z_{GC} = C_{GC} \phi_{GC}(t_{\text{go}}) x_{GC} \tag{44}$$

where

$$\phi_{GC}(t_f, t) = \phi_{GC}(t_{\text{go}}) = \exp(A_{GC} t_{\text{go}}) \tag{45}$$

and

$$C_{GC} = [\,1 \quad 0 \quad 0 \quad 0 \quad 0 \quad 0\,] \tag{46}$$

## IV. Guidance and Control Systems

To demonstrate the advantages of the proposed integrated guidance and control solution for missiles with on–off actuators, we compare it with a two-loop design, where the guidance and control problems are addressed separately. The two designs use SMC in their various components. Moreover, the separate guidance and the integrated solutions use the ZEM in the design.

In the two-loop design, both the missile autopilot inner loop and the outer guidance logic are designed using the SMC methodology. In the sequel, this design is referred to as SMG–SMC (sliding-mode guidance with SMC autopilot). The integrated guidance and control solution, designed using the SMC methodology, is marked as SMGC (sliding-mode-guidance control). The two designs are similar to what was presented in [4], with the proper adjustments to account for the on–off actuator modeling errors and uncertainties. Therefore, here we present only a brief outline.

### A. SMG–SMC Design

The SMC guidance loop design is based on the ZEM variable. Assuming an approximate first-order actuation model, the ZEM has a relative degree of one with respect to the guidance loop output signal $a_{MN}^c$. Therefore, the ZEM defined in Eq. (42) is chosen as the sliding variable.

The SMC guidance design accounts for the bounded modeling errors and target maneuvering uncertainties, given by

$$\dot{a}_{TN} = \left(a_{TN}^c - a_{TN}\right)/\tau_T + \Delta_{aTN} \tag{47a}$$

$$\dot{a}_{MN} = \left(a_{MN}^c - a_{MN}\right)/\tau_M + \Delta_{aMN} \tag{47b}$$

where

$$|\Delta_{aTN}| \le \bar{\Delta}_{aTN}, \qquad |\Delta_{MN}| \le \bar{\Delta}_{aMN} \tag{48}$$

The acceleration command produced by the guidance logic is given by

$$a_{MN}^c = a_{MN}^{\text{eq}} + \frac{\mu_G \text{sign}(Z_G)}{\tau_M \psi(t_{\text{go}}/\tau_M)} \tag{49}$$

where

$$a_{MN}^{\text{eq}} = \frac{\dot{V}_r r}{V_r^2 \tau_M \psi(t_{\text{go}}/\tau_M)} \{V_\lambda + a_{TN}\tau_T[1 - \exp(-t_{\text{go}}/\tau_T)] - a_{MN}\tau_M[1 - \exp(-t_{\text{go}}/\tau_M)]\} \tag{50}$$

and

$$\psi(\zeta) = \exp(-\zeta) + \zeta - 1 \tag{51}$$

To ensure that the sliding surface is reached in a finite time shorter than the interception time $t_{\text{go}}$, we choose $\mu_G$ to be [9]

$$\mu_G \ge \frac{|Z_G|}{t_{\text{go}}} + \bar{\Delta}_{aTNc} + \bar{\Delta}_{aTN\tau} + \bar{\Delta}_{aMN\tau} \tag{52}$$

where the last three elements of the above expression are bounds on the model uncertainties, given by

$$|\tau_T \psi(t_{\text{go}}/\tau_T) a_{TN}^c| \le \bar{\Delta}_{aTNc} \tag{53a}$$

$$|\tau_T^2 \psi(t_{\text{go}}/\tau_T) \Delta_{aTN}| \le \bar{\Delta}_{aTN\tau} \tag{53b}$$

$$|\tau_M^2 \psi(t_{\text{go}}/\tau_T) \Delta_{aMN}| \le \bar{\Delta}_{aMN\tau} \tag{53c}$$

The acceleration command computed above is the input to the autopilot loop, designed to control the missile acceleration

$$a_M = L/m \tag{54}$$

The SMC autopilot is designed using the linear missile model of Eqs. (32–36) with approximate parameters. Therefore, the design model includes modeling errors or uncertainties, assumed to be bounded by

$$|a_M - \bar{a}_M| \le \bar{\Delta}_a \tag{55}$$

where $\bar{a}_M$ is the approximation of the missile acceleration. This error depends also on the difference between the pneumatic and the linear actuator models.

The SMC autopilot is given by

$$\delta^c = \delta^{eq} - \mu \cdot \text{sign}\left(\bar{a}_M - a_M^c\right)/K_\delta \tag{56}$$

where

$$\delta^{eq} = \delta - \frac{K_\alpha}{K_\delta}(q - \bar{a}_M/V_M) \tag{57}$$

$K_\alpha$ and $K_\delta$ are functions of the approximate missile aerodynamics parameters. The controller parameter $\mu$ is chosen to overcome the model uncertainties and the unknown acceleration command rate of change

$$\mu > |K_\alpha/V_M|\bar{\Delta}_a + \bar{\Delta}_{MC} + |K_\delta|\tau_s\bar{\Delta}_\delta \tag{58}$$

Here, $\bar{\Delta}_{MC}$ is the bound on acceleration rate command, defined as

$$|\dot{a}_M^c| \le \bar{\Delta}_{MC} \tag{59}$$

### B. SMGC Design

In the SMGC design, the ZEM of Eq. (44) is used to define the sliding surface. $Z_{GC}$, approximated using the linearized model of Sec. III.C, has a relative degree of 1 with respect to the actuator command $\delta^c$. Therefore, it is chosen as the sliding variable. The subsequent derivations of the SMGC controller use the nonlinear model of Sec. III.A. All the bounded uncertainties of the model are grouped into the bounded $\Delta_{GC}$

$$|\Delta_{GC}| \le \bar{\Delta}_{GC} \tag{60}$$

The SMGC controller is given by

$$\delta^c = \delta^{eq} - \mu_{GC}\text{sign}(Z_{GC})\tau_s/\phi_{GC}^{(1,6)}(t_{\text{go}}) \tag{61}$$

where $\phi_{GC}^{(1,6)}(t_{\text{go}})$ is the (1,6)th element of the numerically computed transition matrix $\phi_{GC}(t_{\text{go}})$ presented in Eq. (45). The equivalent control $\delta^{eq}$ is

$$\delta^{eq} = -\{V_\lambda + a_{TN}\tau_T[1 - \exp(-t_{\text{go}}/\tau_T)] + C_{GC}\phi_{GC}(t_{\text{go}})A_{GC}\bar{x}_{GC}\}\frac{\dot{V}_r r\tau_s}{V_r^2\phi_{GC}^{(1,6)}(t_{\text{go}})} \tag{62}$$

where

$$\bar{x}_{GC} = [0 \quad 0 \quad 0 \quad \alpha \quad q \quad \delta]^T \tag{63}$$

The controller parameter $\mu_{GC}$ is chosen such that the sliding surface is reached in a finite time, shorter than the interception time $t_{\text{go}}$. It is tuned to overcome missile and target dynamics modeling errors and is set to

$$\mu_{GC} > \frac{|Z_{GC}|}{t_{\text{go}}} + \bar{\Delta}_{aTNc} + \bar{\Delta}_{aTN\tau} + \bar{\Delta}_{GC} \tag{64}$$

### C. End-Game Logic Region of Attraction

The guidance and control schemes discussed above treat the very last stage of the interception—the end game. It is preceded by often less accurate midcourse guidance. The purpose of the following analysis is to determine the requirements for the midcourse guidance system that will ensure effective operation of the end-game guidance. These requirements result from the limited maneuverability of the interceptor that is required to cope with agile targets in an uncertain environment. The analysis defines the initial interception conditions for the end-game guidance that will guarantee small miss distances of the target even for the worst case model and target uncertainties. The region of attraction is defined as the subspace of all initial conditions from which the sliding manifold can be reached before interception.

The integrated design was carried out based on the Lyapunov function

$$L_{GC} = \tfrac{1}{2}Z_{GC}^2 \tag{65}$$

To compute the region of attraction we assume that the system is not on the sliding surface $Z_{GC} = 0$. In addition, to attain a maximum maneuver that defines the region of attraction, the canard command is assumed to be at its maximum $|\delta^c| = \delta_{\max}$.

When not on the sliding surface, the canard command, computed by Eq. (61), is dominated by the second attraction term, with $\delta^{eq}$ being practically negligible. This is expressed by

$$|\delta^c| \approx \left|\mu_{GC} \cdot \text{sign}(\sigma_{GC})\tau_s/\phi_{GC}^{(1,6)}(t_{\text{go}})\right| = \delta_{\max} \tag{66}$$

In addition, we require that from the border of the attraction region, the sliding surface could be reached in a finite time, which is shorter than the time to go. This is guaranteed if

$$L_{GC} \le -\dot{L}_{GC} \cdot t_{\text{go}} \tag{67}$$

Substituting Eqs. (65) and (66) into Eq. (67) leads to the region bound equation

$$|Z_{GC}| \le 2\left[\delta_{\max}\frac{|\phi_{GC}^{(1,6)}(t_{\text{go}})|}{\tau_s} - \bar{\Delta}_{aTNc} - \bar{\Delta}_{aTN\tau} - \bar{\Delta}_{GC}\right] \cdot t_{\text{go}} \tag{68}$$

This complex equation will be solved numerically to show the regions of attraction, presented in the following section.

## V. Performance Analysis

Performance of the two guidance and control algorithms derived previously is investigated in this section using numerical simulations. The simulation model incorporated nonlinear kinematics, the nonlinear missile model controlled by a pneumatic actuator, and linear target dynamics.

### A. Scenario

The generic interception setup used in this study is based on the example introduced in [4]. The target performs a square wave ("bang–bang") maneuver with a time period of $\Delta T$ s and a time shift of $\Delta\phi$ s relative to the beginning of the simulation. Simulating the end game only, the initial target-interceptor range was set to 1000 m. The initial velocity vector of the missile is aligned with the initial LOS. The other scenario parameters are as follows:

1) Target velocity is $V_T = 380$ m/s; its maximum acceleration is $a_{T\max} = 20$ g; the maneuvering lag time constant varies in the range $\tau_T = [0.05, 0.15]$ s; the maneuver period is $\Delta T = 1$ s; the maneuver time shift $\Delta\phi$ is selected randomly between zero and $\Delta T$.

2) Missile velocity is $V_M = 380$ m/s. For its approximate first-order dynamics in Eq. (30), a time constant of $\tau_M = 0.1$ s is assumed. The missile aerodynamic model parameters are

$$\bar{L}_\alpha^B = 1190\ [\text{m/s}^2], \qquad \bar{L}_\alpha^\delta = 80\ [\text{m/s}^2] \qquad \bar{M}_\alpha^B = -260\ [1/\text{s}^2]$$
$$\bar{M}_q = -5\ [1/\text{s}], \qquad \bar{M}_\alpha^\delta = 160\ [1/\text{s}^2]$$

These values are used in the controller design only. To simulate aerodynamics uncertainties, the missile simulation parameters differ from the model above by as much as $\pm 20\%$.

3) The parameters of the pneumatic actuator were presented in Sec. III.B. It is assumed that thermodynamically the process in the piston is polytropic with a nominal process parameter $n = 1.45$. The

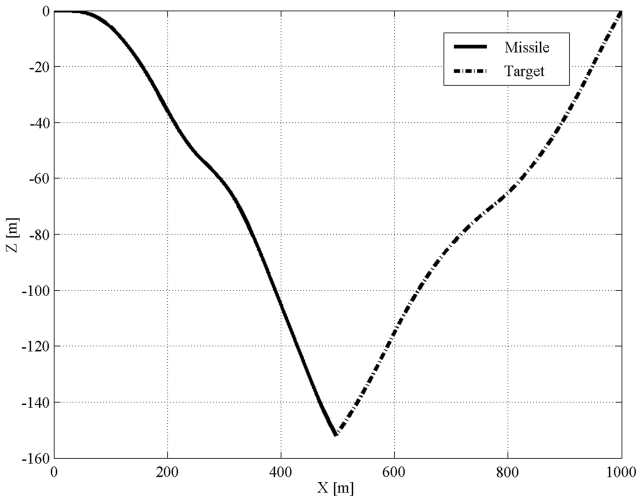


**Fig. 7 Sample run trajectories.**

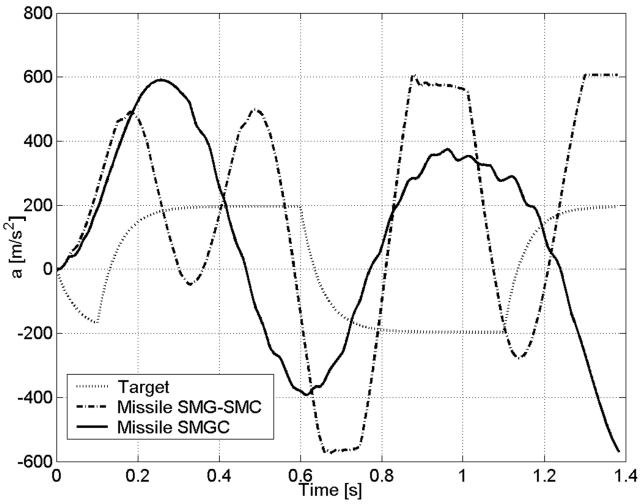


**Fig. 9 Target and missile acceleration profiles for a sample run.**

actuator commands are limited by $\delta^c_{\max} = 30$ deg. The time constant of its first-order approximation model was set to $t_s = 0.01$ s.

The initial interceptor and target flight path angles are $\gamma^0_M = 0$ deg and $\gamma^0_T = 160$ deg, respectively, whereas their initial acceleration is set to zero, $a^0_M = a^0_T = 0$. The engagement trajectories for a sample run are plotted in Fig. 7.

### B. Sample Run Performance

In this section we examine the performance of the two designs for a sample run. The target parameters are $\tau_T = 0.05$ s and $\Delta\phi = 0.1$ s. The simulation includes the pneumatic actuator model.

The ZEMs for these runs are plotted in Fig. 8. Although in both cases the ZEM is reduced drastically in the first part of the solution, the integrated design maintains much smaller ZEM values also after the initial transient compared to the two-loop design. This will favorably affect the average interception performance, as will be shown in the sequel. The target acceleration together with the missile acceleration profiles for the two designs are plotted in Fig. 9. This figure demonstrates that the improved performance advocated for the integrated design is achieved without a significant increase of the missile maneuver effort.

Figures 10 and 11 compare the canard motion for the two designs. Contrary to the integrated solution, in the two-loop design the canard is saturated most of the time. On the other hand, the integrated design exhibits a more dynamic, fluctuating behavior, required to better reduce the ZEM (see Fig. 8).

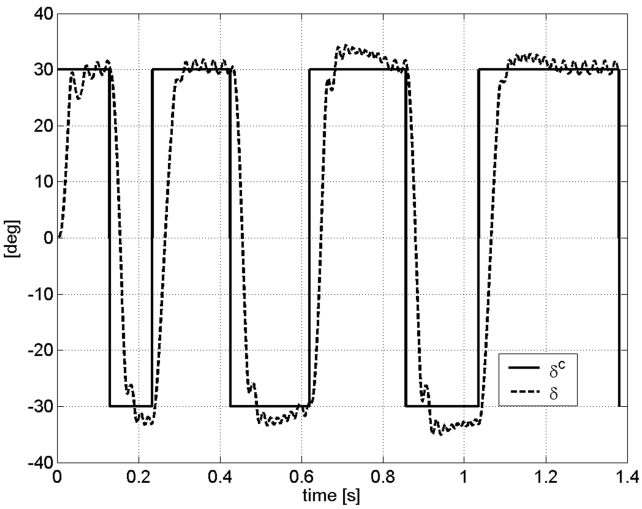


**Fig. 10 Sample run: $\delta$ and $\delta^c$ for the two-loop design.**

### C. Homing Performance

The homing performance of the different algorithms is evaluated using a Monte Carlo study. In these runs, the target maneuver phase was varied in the range 0–1 s between different runs. The

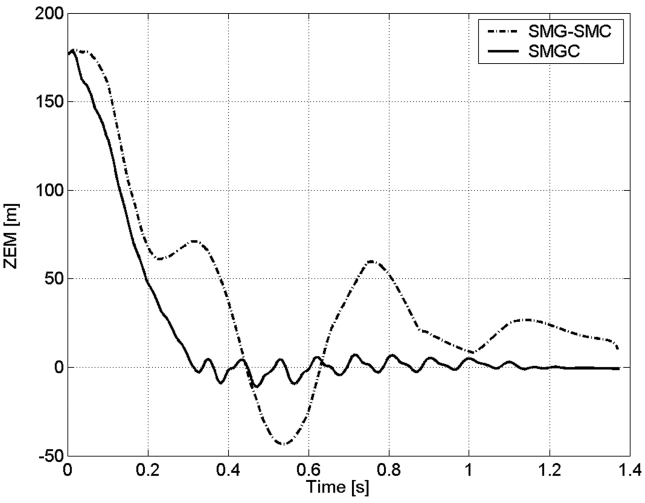


**Fig. 8 ZEM comparison for a sample run.**

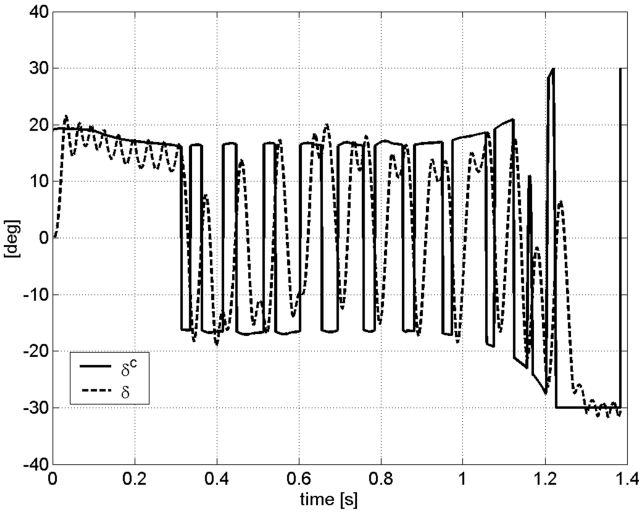


**Fig. 11 Sample run: $\delta$ and $\delta^c$ for the integrated design.**

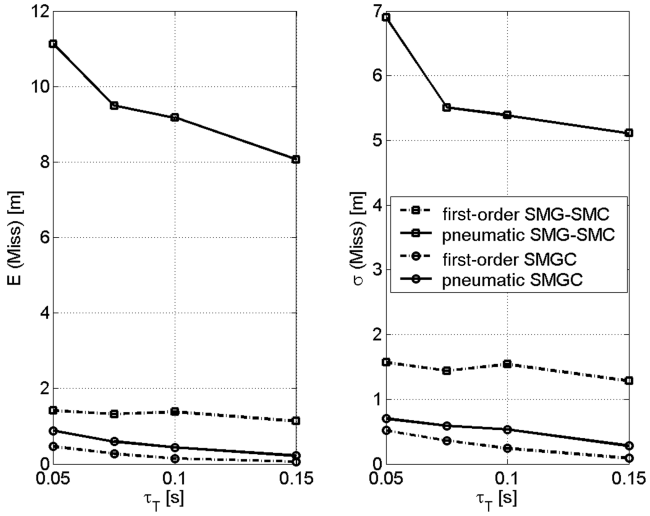


**Fig. 12 Monte Carlo study: average and standard deviation of the miss distance.**

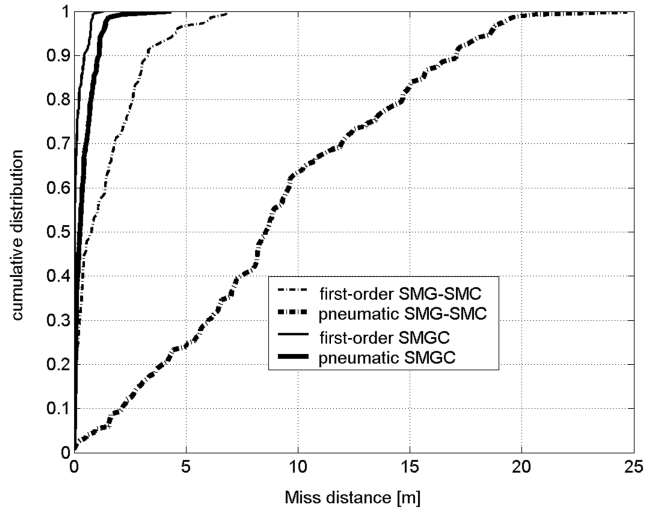


**Fig. 13 Monte Carlo study: cumulative distribution of the miss distance for a target with $\tau_T = 0.1$ s.**

Monte Carlo test points are characterized by the target time constant $\tau_T$ that varies in the range 0.05–0.15 s. Each point consists of 150 runs. Figure 12 presents the average $E$ and the standard deviation $\sigma$ of the interception miss distances for the integrated and the two-loop designs. For comparison, we show also the results obtained using a linear actuator. In a slightly different form, Fig. 13 depicts the cumulative distribution of the miss distance for the various guidance schemes and actuator models, and a target time constant of $\tau_T = 0.1$ s.

These results clearly demonstrate the superior performance of the integrated design. In both designs the performance is degraded when a pneumatic (oscillating) actuator is used instead of a linear one. In addition, larger miss distances are attained for high bandwidth targets, characterized by small values of $\tau_T$. However, the integrated design shows a dramatically lower sensitivity to the actuation characteristics and the control surface oscillations. For example, as can be seen in Fig. 13, the SMG–SMC guidance and control scheme demonstrates that 90% of the runs end with miss distances that are lower than 3.3 m for a missile with linear actuation, increasing to 17 m when a pneumatic actuator is used. The integrated SMCG logic shows that with a linear actuator 90% of runs end with a miss distance smaller than approximately 0.46 m. With pneumatic actuators this distance increases to about 1.12 m, significantly lower than the result with SMG–SMC. These favorable results of the integrated design are accredited to the robustness of the SMC method and the integrated model used in the design.

**Table 1 Monte Carlo simulation results for different types of the thermodynamic process in the cylinder**

| $n$ | $E$ (miss), m | $\sigma$ (miss), m |
|---|---|---|
| 1 (isothermal process) | 0.51 | 0.51 |
| 1.23 | 0.46 | 0.45 |
| 1.45 | 0.44 | 0.53 |
| 1.67 ($=\gamma$, isentropic) | 0.43 | 0.47 |

### D. Sensitivity to the Thermodynamic Model Uncertainty

In this section we examine the sensitivity of the homing performance to parametric uncertainties in the model of the pneumatic actuator. In particular, we examine the effect of the thermodynamic process model of the gas flow in the cylinder, which was assumed to be polytropic. In the simulation, the process is varied from isothermal to isentropic by varying the parameter $n$ of the polytropic model in Eq. (16) from 1 (isothermal) to $\gamma$ (isentropic). The Monte Carlo runs for the integrated design (SMGC) were carried out for a target with $\tau_T = 0.1$ s.

Table 1 present the average $E$ and the standard deviation $\sigma$ of the results for 150 Monte Carlo runs. The results show only small variations in the system performance when tested with different types of the thermodynamic process. This further demonstrates the robustness of the integrated SMGC design.

### E. End-Game Regions of Attraction

For the engagement scenario discussed here, we computed the attraction region of the integrated end-game guidance and control logic. The boundary of this region was defined in Eq. (68). It depends on many parameters: the state space vector of the integrated problem, $x_{GC} = [z \quad \dot{z} \quad a_{TN} \quad \alpha \quad q \quad \delta]^T$, the initial engagement geometry (flight path angles and range), and the estimated time to go. To simplify the problem, we assume no target acceleration command, no interceptor maneuvering, and zero line of sight angle

$$a_{TN}^c = \alpha = q = \delta = z = 0 \tag{69}$$

With these assumptions, the equality in Eq. (68) depends only on the three remaining parameters: the range and flight path angles. Thus, for fixed initial range $R_0$ and interceptor flight path angle $\gamma_M$, we search numerically for the target flight path angle $\gamma_T$ so that Eq. (68) holds. The resulting regions of attraction are shown in Fig. 14 for various initial ranges.

Several conclusions can be drawn when analyzing the plots in Fig. 14. First, as expected, the region of attraction shrinks as the range to the target is reduced. Moreover, below a certain range, in our case for $R_0$ less than 116 m, only "tail chaise" configurations can guarantee interception. Short range "head-on" interception cannot be guaranteed because, due to a higher closing velocity and hence shorter interception times, worst case target maneuvers and model uncertainties cannot be balanced by the maximum canard deflections. All the regions are bounded on the right and left by straight lines, beyond which the initial closing velocity is negative. Commonly, negative closing velocity defines the end of an interception, and thus is considered to be outside the attraction region in this analysis. In head-on scenarios, obtained when $\gamma_M$ is around zero and $\gamma_T$ around 180 deg, for small ranges the region of attraction approaches a collision triangle, given in this case by a line with a slope of $-1$ and crossing the point (0, 180) in the $\gamma_M$ vs $\gamma_T$ plot (see, for example, the attraction region for $R_0 = 150$ m).

## VI. Conclusions

This paper demonstrates the performance superiority of an integrated guidance and control design for missiles with pneumatic on–off actuators. The most noticeable feature of this design is its low sensitivity and robustness with respect to actuator model

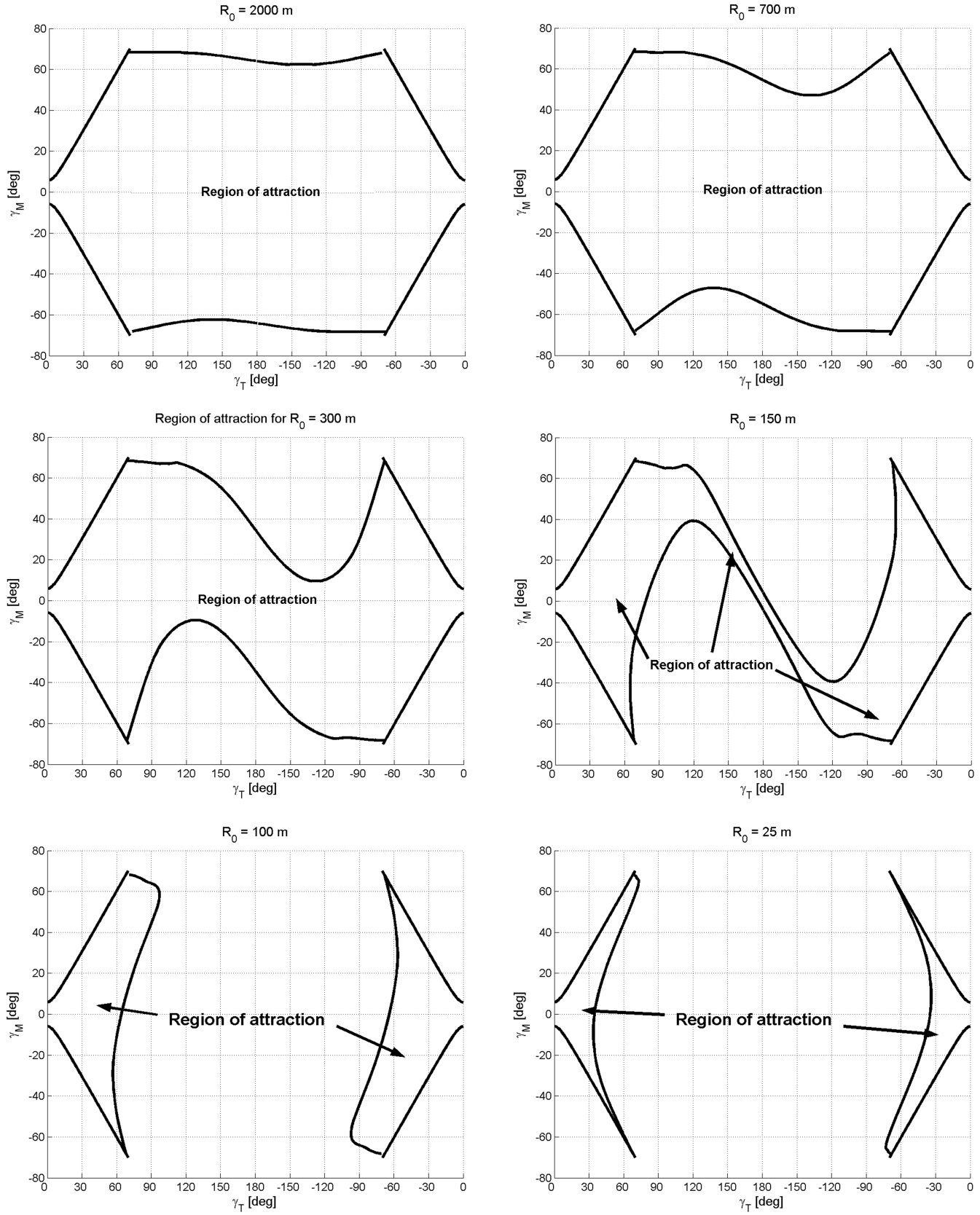


**Fig. 14 End-game regions of attraction for various initial ranges.**

characteristics. Simulation results with the integrated design show only minor performance degradation of a pneumatically actuated missile compared to one controlled by a linear actuator. This paper also provides accuracy requirements for midcourse guidance algorithms, to ensure that once engaged the integrated end-game logic can provide high interception accuracy.

## References

[1] Lin, C. F., Wang, Q., Speyer, J. L., Evers, J. H., and Cloutier, J. R., "Integrated Estimation, Guidance, and Control System Design Using Game Theoretic Approach," *Proceedings of the American Control Conference*, American Automatic Control Council, Evanstone, IL, 1992, pp. 3220–3224.

[2] Palumbo, N. F., and Jackson, T. D., "Integrated Missile Guidance and Control: A State Dependent Riccati Differential Equation Approach," *Proceeding of the IEEE International Conference on Control Applications*, IEEE, Piscataway, NJ, 1999, pp. 243–248.

[3] Menon, P. K., and Ohlmeyer, E. J., "Nonlinear Integrated Guidance-Control Laws for Homing Missiles," *Proceeding of the AIAA Guidance, Navigation, and Control Conference*, CP-4160, AIAA, Washington, D. C., 2001.

[4] Shima, T., Idan, M., and Golan, O. M., "Sliding Mode Control for Integrated Missile Autopilot-Guidance," *Journal of Guidance, Control, and Dynamics*, Vol. 29, No. 2, March–April 2006, pp. 250–260.

[5] Idan, M., Shima, T., and Golan, O. M., "Integrated Sliding Mode Autopilot-Guidance for Dual Control Missiles," *Journal of Guidance, Control, and Dynamics*, Vol. 30, No. 4, July–Aug. 2007, pp. 1081–1089.
doi:10.2514/1.24953

[6] Shkolnikov, I., Shtessel, Y. B., Lianos, D., and Thies, A. T., "Robust Missile Autopilot Design via High-Order Sliding Mode Control," *Proceeding of the AIAA Guidance, Navigation, and Control Conference*, CP-3968, AIAA, Washington, D.C., 2000.

[7] Moon, J., and Kim, Y., "Design of Missile Guidance Law via Variable Structure Control," *Proceeding of the AIAA Guidance, Navigation, and Control Conference*, CP-4068, AIAA, Washington, D.C., 2000.

[8] Utkin, V. I., *Sliding Modes in Control and Optimization*, Springer–Verlag, Berlin, 1992.

[9] Slotine, J.-J. E., and Li, W., *Applied Nonlinear Control*, Prentice–Hall, Upper Saddle River, NJ, 1991, pp. 276–307, Chap. 7.

[10] Zarchan, P., *Tactical and Strategic Missile Guidance*, Progress in Astronautics and Aeronautics, Vol. 176, AIAA, Washington, D.C., 1997, pp. 20–28.

[11] Hatsopoulos, G. N., and Keenan, J. H., *Principles of General Thermodynamics*, Krieger, Malabar, FL, 1981, pp. 222–223.

[12] Shavit, A., and Gutfinger, C., *Thermodynamics, from Concepts to Applications*, Prentice–Hall, Upper Saddle River, NJ, 1995, pp. 72–73.

[13] Shapiro, A. H., *The Dynamic and Thermodynamics of Compressible Fluid Flow*, Vol. 1, Ronald, New York, 1953, pp. 112–189, Chaps. 5–6.